Draft version January 3, 2018
Preprint typeset using LaTeX style AASTeX6 v. 1.0

SHORT-LIVED CIRCUMSTELLAR INTERACTION IN THE LOW-LUMINOSITY TYPE IIP SN 2016bkv

Griffin Hosseinzadeh[1,2], Stefano Valenti[3], Curtis McCully[1,2], D. Andrew Howell[1,2], Iair Arcavi[1,2,10], Anders Jerkstrand[4], David Guevel[1,2,5], Leonardo Tartaglia[3,6], Liming Rui (芮黎明)[7], Jun Mo (莫军)[7], Xiaofeng Wang (王晓锋)[7], Fang Huang (黄芳)[7], Hao Song (宋浩)[7], Tianmeng Zhang (张天萌)[8], and Koichi Itagaki (板垣公一)[9]

[1] Las Cumbres Observatory, 6740 Cortona Dr Ste 102, Goleta, CA 93117-5575, USA; griffin@lco.global
[2] Department of Physics, University of California, Santa Barbara, CA 93106-9530, USA
[3] Department of Physics, University of California, 1 Shields Ave, Davis, CA 95616-5270, USA
[4] Max-Planck-Institut für Astrophysik, Karl-Schwarzschild-Straße 1, D-85748 Garching, Germany
[5] Harvard-Smithsonian Center for Astrophysics, 60 Garden Street, Cambridge, MA 02138-1516, USA
[6] Department of Astronomy/Steward Observatory, 933 North Cherry Avenue, Tucson, AZ 85721-0065, USA
[7] Physics Department and Tsinghua Center for Astrophysics, Tsinghua University, Beijing, 100084, China
[8] National Astronomical Observatory of China, Chinese Academy of Sciences, Beijing, 100012, China
[9] Itagaki Astronomical Observatory, Yamagata 990-2492, Japan

ABSTRACT

While interaction with circumstellar material is known to play an important role in Type IIn supernovae (SNe), analyses of the more common SNe IIP and IIL have not traditionally included interaction as a significant power source. However, recent campaigns to observe SNe within days of explosion have revealed narrow emission lines of high-ionization species in the earliest spectra of luminous SNe II of all subclasses. These "flash ionization" features indicate the presence of a confined shell of material around the progenitor star. Here we present the first low-luminosity SN to show flash ionization features, SN 2016bkv. This SN peaked at $M_V = -16$ mag and has Hα expansion velocities under 1350 km s^{-1} around maximum light, placing it at the faint/slow end of the distribution of SNe IIP (similar to SN 2005cs). The light curve shape of SN 2016bkv is also extreme among SNe IIP. A very strong initial peak indicates a significant fraction of the luminosity comes from circumstellar interaction. A very small fall from the plateau to the nickel tail indicates unusually large production of radioactive nickel compared to other low-luminosity SNe IIP. Comparing nebular spectra of SN 2016bkv to models suggests that it came from a low-mass red supergiant progenitor. As such, we discuss the possibility that SN 2016bkv is an electron-capture supernova.

Keywords: supernovae: general — supernovae: individual (SN 2016bkv)

1. INTRODUCTION

The majority of massive ($M_{\rm ZAMS} \gtrsim 8$ M$_\odot$) stars end their lives as Type II supernovae (SNe), i.e., those with hydrogen-rich spectra (Smartt 2009; Arcavi 2017). Broadly speaking, SNe II can be divided into two subclasses. SNe IIP/L have light curves that plateau (P) or decline linearly (L) for roughly 100 days before falling to a radioactive-decay-powered tail (Barbon et al. 1979). SNe IIn have spectra domniated by narrow (n) hydrogen emission lines, indicating strong interaction with circumstellar material (CSM; Schlegel 1990; Chugai 1991). Hereinafter we will use "SNe II" to refer to SNe IIP and IIL as a single class, excluding SNe IIb and IIn.

SNe II peak in the range $-14 \gtrsim M_B \gtrsim -18$ mag (Patat et al. 1994) and show a correlation between plateau luminosity and photospheric expansion velocities (Hamuy & Pinto 2002; Pejcha & Prieto 2015). Pumo et al. (2017) claim that the ratio of the explosion energy to the ejected mass controls the plateau luminosity of SNe II, where smaller ratios are less luminous (see their Figure 5). At the faint/slow end of this distribution is a group of events referred to as low-luminosity (LL) SNe II (Pastorello et al. 2004; Spiro et al. 2014), exemplified by the nearby, well-studied SN 2005cs, whose red supergiant (RSG) progenitor star was detected by Maund et al. (2005) and Li et al. (2006) in pre-explosion images taken by the *Hubble Space Telescope* (*HST*). Several models have been proposed to explain LL SNe II, including high-mass RSGs exploding as fallback SNe (Turatto et al. 1998; Zampieri et al. 1998) and low-mass RSGs exploding as electron-capture SNe (Chugai & Utrobin 2000).

Interaction with CSM traditionally has not been con-

[10] Einstein Fellow

sidered significant in SNe II, since broad P Cygni lines dominate their spectra. However, recent efforts to obtain spectra of SNe within days of explosion have resulted in the discovery of narrow emission features in a significant fraction of early spectra of SNe II (18% of those observed within 5 days of explosion; Khazov et al. 2016). Early examples of these features include SNe 1983K (Niemela et al. 1985), 1993J (Benetti et al. 1994; Garnavich & Ann 1994; Matheson et al. 2000), 1998S (Leonard et al. 2000; Shivvers et al. 2015), and 2006bp (Quimby et al. 2007). Gal-Yam et al. (2014) first coined the term "flash spectroscopy" to describe this emission, produced as the CSM recombines after being ionized by the initial shock breakout flash. More recently, Yaron et al. (2017) observed flash spectra of the Type II SN 2013fs changing on hour time scales.

Intriguingly, Khazov et al. (2016) suggest that the presence of flash ionization features may be correlated with luminosity; in fact, all their flash ionization spectra are from events with peak absolute magnitudes $M_R < -17.5$ mag. This implies that more luminous events maintain higher temperatures at early times, enabling high-ionization lines to persist in their spectra long enough to be detected.

The object presented here, SN 2016bkv, is a SN II discovered soon after explosion. With a peak absolute magnitude of $M_V = -16$ mag and Hα expansion velocities under 1350 km s^{-1}, it greatly resembles SN 2005cs and other LL events in the literature. However, unlike any previous LL SN II, its pre-maximum spectra are dominated by narrow emission lines from high-ionization species, making it the least luminous SN for which flash ionization of the CSM has been detected. Below we report observations of SN 2016bkv and discuss their implications for the role of CSM interaction in SNe II. We also investigate the progenitor of SN 2016bkv, in particular whether it exploded due to iron core collapse or electron capture.

2. DISCOVERY

Itagaki (2016) discovered SN 2016bkv on 2016 March 21.70 UT at 17.5 mag using an unfiltered Celestron 14 inch (35 cm) telescope. Ross et al. (2016) do not detect the supernova on March 19.29, but only to an unfiltered limiting magnitude of 17 mag. Since this limit is not as deep as the first detection, in order to determine the explosion time, we fit $F(t) = F_1(t - t_0)^2$ to the first three unfiltered photometry points, after which the light curve appears to rise more slowly. This yields March 20.5 (MJD$_0$ = 57467.5 ± 1.2) as the explosion epoch, where we have adopted the time between estimated explosion and first detection as the uncertainty. Coindicentally, this uncertainty range includes the entire period from nondetection to first detection. Hosseinzadeh et al. (2016) obtained the first spectrum on March 23.5, classifying the transient as a young SN II.

At right ascension $10^{\rm h}18^{\rm m}19\overset{\rm s}{.}31$ and declination $+41°25'39\overset{''}{.}3$ (J2000), SN 2016bkv lies $30\overset{''}{.}3$ (2.11 kpc projected) from the center of the spiral galaxy NGC 3184, which has a redshift of $z = 0.001975 \pm 0.000003$ (Strauss et al. 1992) and a Cepheid-based distance modulus of $\mu = 30.79 \pm 0.05$ mag (Ferrarese et al. 1999)[11], corresponding to a luminosity distance of $d_L = 14.4 \pm 0.3$ Mpc. In the past century, NGC 3184 has hosted at least four other SNe—1921B, 1921C, 1937F (Shapley 1939)[12], and 1999gi (Type II; Schlegel 2001; Smartt et al. 2001)—and one SN impostor—2010dn, which Smith et al. (2011) identify as the outburst of a luminous blue variable star.

As noted by Milisavljevic et al. (2016), images of NGC 3184 from *HST* show a star cluster at the position of SN 2016bkv. When the SN fades, it may be possible to determine the luminosity and colors of the progenitor star based on the change in flux from the cluster.

3. OBSERVATIONS AND DATA REDUCTION

In addition to unfiltered photometry from the 35 and 60 cm telescopes at Itagaki Astronomical Observatory (Yamagata, Japan), we obtained *UBVgri* photometry of SN 2016bkv using Las Cumbres Observatory's (Brown et al. 2013) robotic 1 m telescope located at the McDonald (TX, USA) Observatory and *UBVRI* photometry using the 0.8 m Tsinghua University–National Astronomical Observatory of China Telescope (TNT; Huang et al. 2012) located at Xinglong Observatory (Hebei Province, China). Unfortunately, the *Swift* satellite could not observe the SN in ultraviolet due to a nearby bright star.

Photometry measurements were complicated by the fact that the SN occurred in a bright but unresolved H II region (number 62 in the list of Hodge & Kennicutt 1983) and about 7.7" away from an even brighter star (SDSS J101819.82+412544.3; Adelman-McCarthy et al. 2007). We obtained *BVgri* reference images with Las Cumbres approximately 600 days after explosion, when the SN was much fainter than the H II region, and subtracted them from the images of the supernova using PyZOGY (Guevel & Hosseinzadeh 2017), a new open-source Python image subtraction pipeline based on the optimal algorithm of Zackay et al. (2016). We then measured aperture photometry on the difference images using `lcogtsnpipe` (Valenti et al. 2016). The *U*-band light curve is PSF photometry on unsubtracted images,

[11] Note, however, that other methods give distance moduli ranging from 29.3 mag (Pierce 1994) to 31.2 mag (Jones et al. 2009).

[12] Spectra of these SNe from E. Hubble's and F. Zwicky's programs were never obtained, but they have been photometrically classified as Types II, I, and IIP, respectively (Barbon et al. 2008).

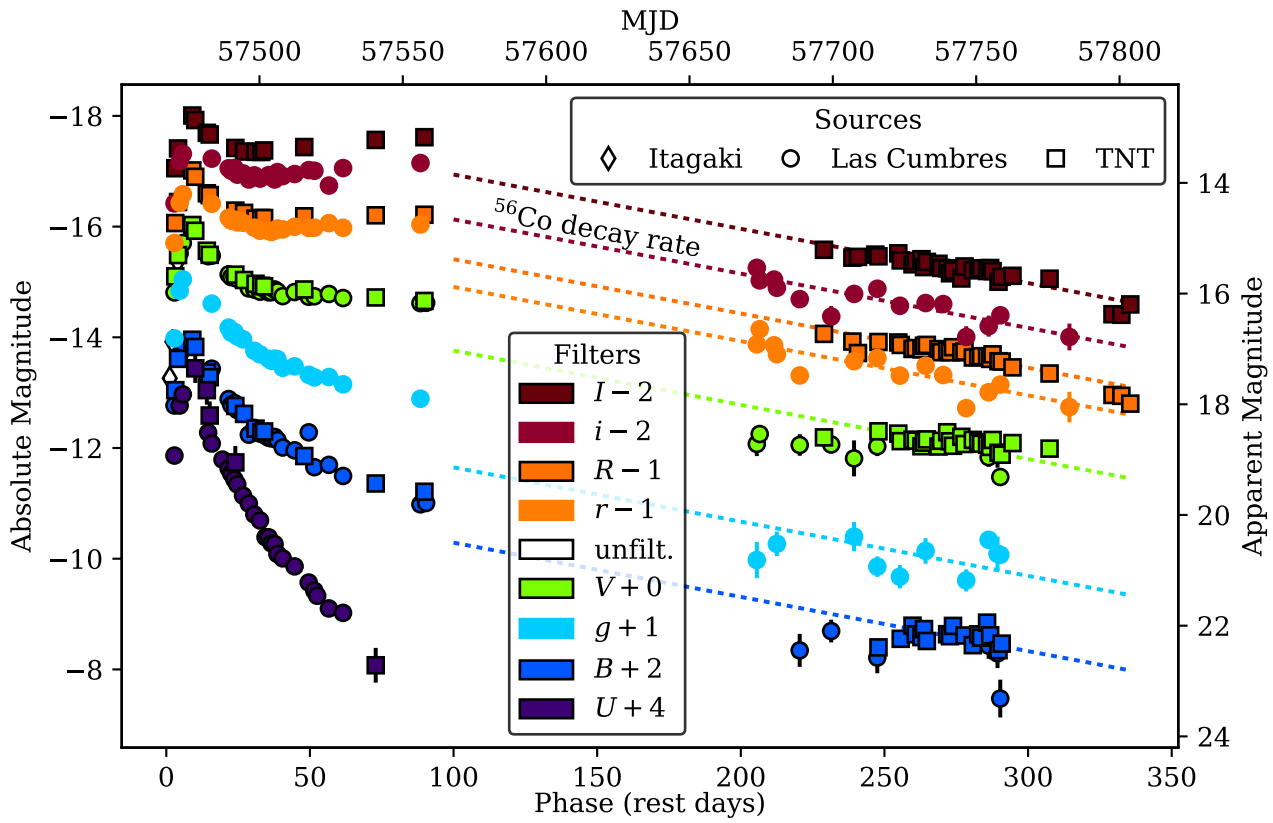

Figure 1. One year of photometry of SN 2016bkv. Late nondetections are hidden for clarity. Note the strong early bump and the small fall from plateau, which happened while the supernova was behind the sun. (The data used to create this figure are available.)

because host contamination in our reference images is much weaker in U. *UBV* photometry is calibrated in the Vega system to Landolt (1992) standard fields observed on the same night as the SN. *gri* photometry is calibrated in the AB system to stars in the Sloan Digital Sky Survey Data Release 8 (SDSS DR8; Aihara et al. 2011).

We obtained a U-band reference image with TNT approximately 300 days after explosion and *BVRI* references approximately 600 days after explosion. We subtracted these from the TNT images of the supernova using HOTPANTS (Becker 2015) and measured PSF photometry using a custom pipeline based on PyRAF tasks (Science Software Branch at STScI 2012). TNT *UBVRI* photometry is calibrated in the Vega system to SDSS DR13 stars (Albareti et al. 2017).

We measured PSF photometry from the remaining unsubtracted images using standard PyRAF tasks. Unfiltered photometry is calibrated to 20 nearby stars in SDSS DR6 (Adelman-McCarthy et al. 2007) by fitting blackbody spectra to their *ugriz* photometry and, for stars with reasonable fits, convolving the spectra with the spectral response curve of K. Itagaki's KAF-1001E CCD (both telescopes use the same CCD) to produce AB magnitudes. The resulting unfiltered magnitudes are not relevant to the bolometric light curve we produce in Section 4.2, but we do consider them when fitting the early light curve in Section 4.3. The photometry is plotted in Figure 1.

We obtained 17 optical spectra of SN 2016bkv during the flash-ionization (Figure 2) and photospheric (Figure 3) phases using the robotic FLOYDS instrument, mounted on Las Cumbres Observatory's 2 m telescope on Haleakalā (HI, USA), and the Beijing Faint Object Spectrograph and Camera (BFOSC) and the Optomechanics Research Inc. (OMR) low-resolution spectrograph, both mounted on the 2.16 m telescope at Xinglong (Fan et al. 2016). Note that these low-resolution spectrographs cannot resolve lines with velocities below ~ 800 km s^{-1}, meaning that we cannot constrain the photospheric velocity of SN 2016bkv during most of its evolution. Four additional spectra were obtained during the nebular phase using the Kast Double Spectrograph (Miller & Stone 1994) on the C. Donald Shane Telescope at Lick Observatory (CA, USA) and the Low-Resolution Imaging Spectrometer (LRIS; Oke et al. 1995; Rockosi et al. 2010) on the Keck I telescope at the W. M. Keck Observatory (HI, USA). All spectra are logged in Table 1 and available for download from the Weizmann Interactive Supernova Data Repository (Yaron & Gal-

Yam 2012).

Table 1. Log of Spectroscopic Observations

MJD	Telescope	Instrument	Phase (d)
57470.5	Las Cumbres 2 m	FLOYDS	3.0
57471.4	Las Cumbres 2 m	FLOYDS	3.9
57471.6	Xinglong 2.16 m	BFOSC	4.1
57472.3	Las Cumbres 2 m	FLOYDS	4.8
57475.3	Las Cumbres 2 m	FLOYDS	7.8
57480.4	Las Cumbres 2 m	FLOYDS	12.9
57481.6	Xinglong 2.16 m	BFOSC	14.0
57487.4	Las Cumbres 2 m	FLOYDS	19.9
57491.6	Xinglong 2.16 m	BFOSC	24.0
57492.4	Las Cumbres 2 m	FLOYDS	24.9
57498.4	Las Cumbres 2 m	FLOYDS	30.8
57502.3	Las Cumbres 2 m	FLOYDS	34.7
57507.3	Las Cumbres 2 m	FLOYDS	39.7
57511.3	Las Cumbres 2 m	FLOYDS	43.7
57514.6	Xinglong 2.16 m	OMR	47.0
57526.3	Las Cumbres 2 m	FLOYDS	58.6
57550.3	Las Cumbres 2 m	FLOYDS	82.6
57724.6	Shane	Kast	256.6
57780.4	Shane	Kast	312.2
57903.3	Keck I	LRIS	434.9
58075.6	Keck I	LRIS	606.9

4. ANALYSIS

4.1. *Flash Spectroscopy*

Initially, the spectrum of SN 2016bkv shows narrow emission lines of hydrogen (410.1, 434.0, 486.1, and 656.3 nm), He II (468.6 and 541.1 nm), C III (464.8 and 569.6 nm), N III (464.0 nm), and possibly O II (371.3–374.9 nm). With the exception of O II, these lines are a subset of those identified by Gal-Yam et al. (2014) in the Type IIb SN 2013cu (modeled by Groh 2014) and by Yaron et al. (2017) in the Type II SN 2013fs. The line widths are likely unresolved by our low-resolution spectrographs.

Previously, only three LL SNe II were observed spectrally this soon after explosion: SNe 2002gd (Faran et al. 2014; Spiro et al. 2014), 2005cs (Pastorello et al. 2006; Faran et al. 2014), and 2010id (Gal-Yam et al. 2011). Although their spectra are similarly blue, none of them show narrow emission features, instead being dominated by the same P Cygni profiles as during the photospheric phase (see Figure 2). Notably, Gal-Yam et al. (2014)

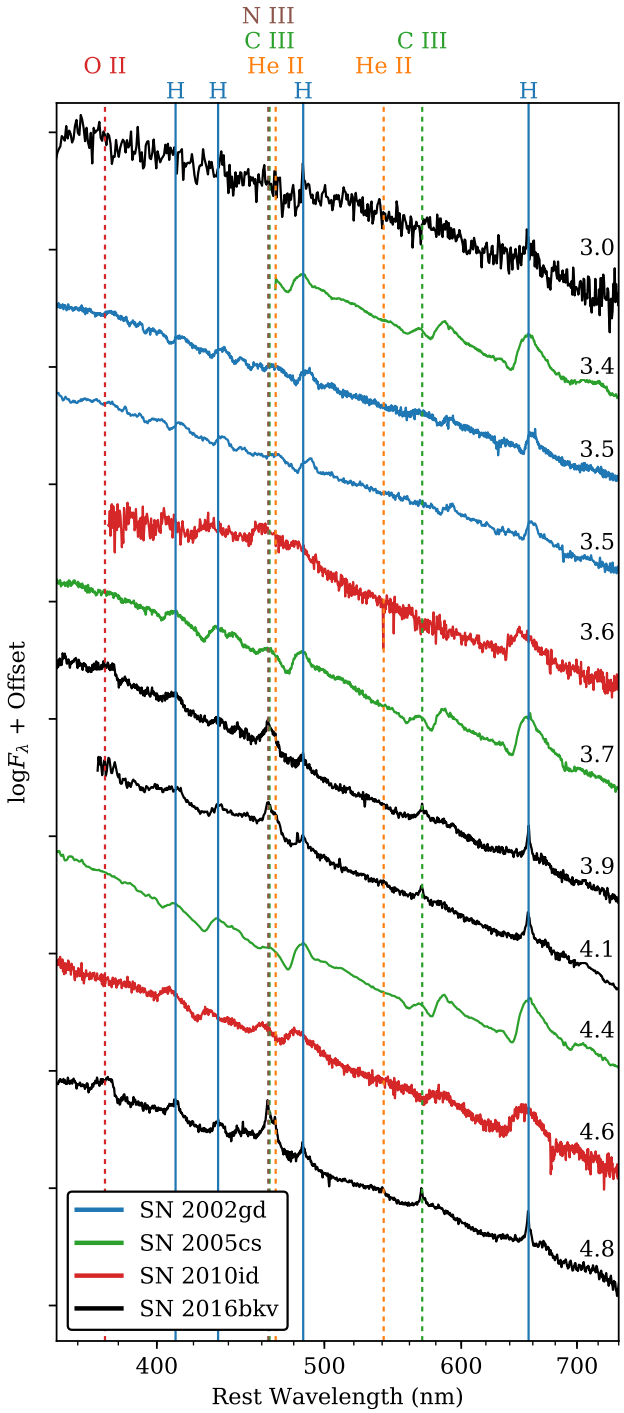

Figure 2. Flash-ionized spectra of SN 2016bkv compared with all spectra of LL SNe II observed within five days of estimated explosion: SNe 2002gd (Faran et al. 2014; Spiro et al. 2014), 2005cs (Pastorello et al. 2006; Faran et al. 2014), and 2010id (Gal-Yam et al. 2011). Phases in days from estimated explosion are marked to the right of each spectrum. SN 2016bkv is the only one that shows narrow emission of high-ionization species (dotted vertical lines).

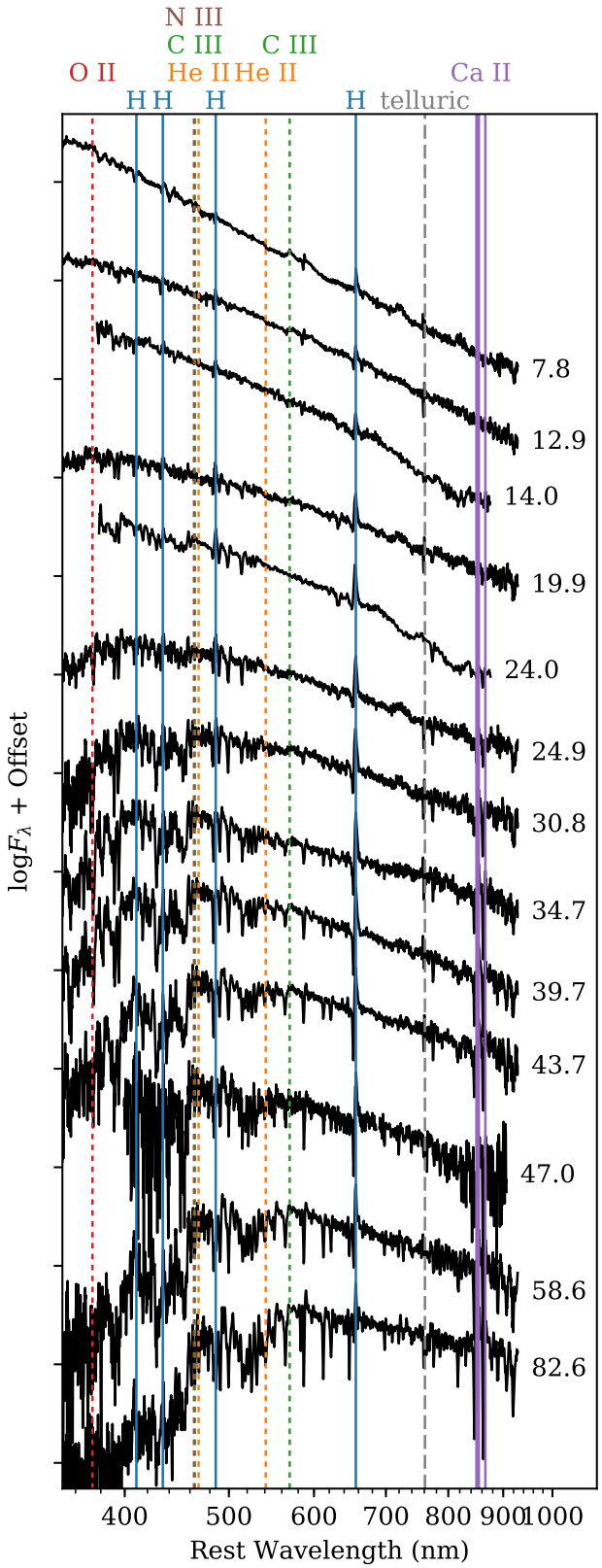

Figure 3. Photospheric spectra of SN 2016bkv; see Figure 7 for a more detailed line identification during the photospheric phase. Phases in days from estimated explosion are marked to the right of each spectrum. The early high-ionization lines in Figure 2 disappear after 5 days, giving way to typical SN II spectra with very low photospheric velocities (Hα velocity $< 1350\,\mathrm{km\,s^{-1}}$).

identify a feature around 468 nm as He II, an indicator of very high temperatures, in their second spectrum of SN 2010id. However, Pastorello et al. (2004) identify a similar feature as high-velocity Hβ in their spectra of SN 2005cs (see their Figure 5).

Because of the very low photospheric velocity of SN 2016bkv, lower than these other three events, we suggest that its CSM may have lasted longer before being swept up by supernova ejecta. This would have made flash spectroscopy easier by allowing us more time after explosion to observe the narrow emission lines. A larger sample size of well-observed flash-ionized SNe II would allow us to search for a correlation between photospheric velocity and duration of flash spectra.

4.2. *Blackbody Fitting and Bolometric Light Curve*

We construct a bolometric light curve of SN 2016bkv by fitting each epoch of photometry with a blackbody spectrum. In order to compare to bolometric light curves from the literature, typically constructed using only optical photometry, we then integrate the blackbody spectrum from U to I. The result is shown in Figure 4, where it is compared to bolometric light curves of other SNe II from Valenti et al. (2016).

The bolometric light curve of SN 2016bkv is extreme in two ways. First, it has a very strong peak around 7 days after explosion with respect to the plateau luminosity ($s1$ in Valenti et al. 2016). We attribute this to excess luminosity from circumstellar interaction. Second, it has a very small fall between the plateau and the radioactive nickel tail (assuming a typical 100 d plateau). This implies that the amount of nickel produced in the explosion is unusually large for a LL SN II. Comparing the luminosity on the tail to SN 1987A as in Hamuy (2003), we find that SN 2016bkv produced $M_{\mathrm{Ni}} = 0.0216 \pm 0.0014\,M_\odot$ of nickel. The uncertainty in this measurement is almost entirely due to the 2% uncertainty on the distance to the supernova, the 5% assumed uncertainty on the host-galaxy extinction ($A_V = 0.00 \pm 0.05$ mag), and the 1.2% uncertainty from the explosion epoch.

This measurement is surprisingly higher than for previous LL SNe IIP and merits a careful consideration of the uncertainties. If supernova light was still present in the reference images we used to create our subtracted light curve, the luminosity we derived would be lower than the true luminosity, making the nickel mass even higher. Likewise, if extinction from dust in the ejecta were important, the true underlying luminosity would be higher than we observe, again making the nickel mass higher. In order to get a nickel mass similar to other LL SNe IIP, the true luminosity would have to be about 3 times lower than what we observe.

Figure 5 shows the evolution of the blackbody temper-

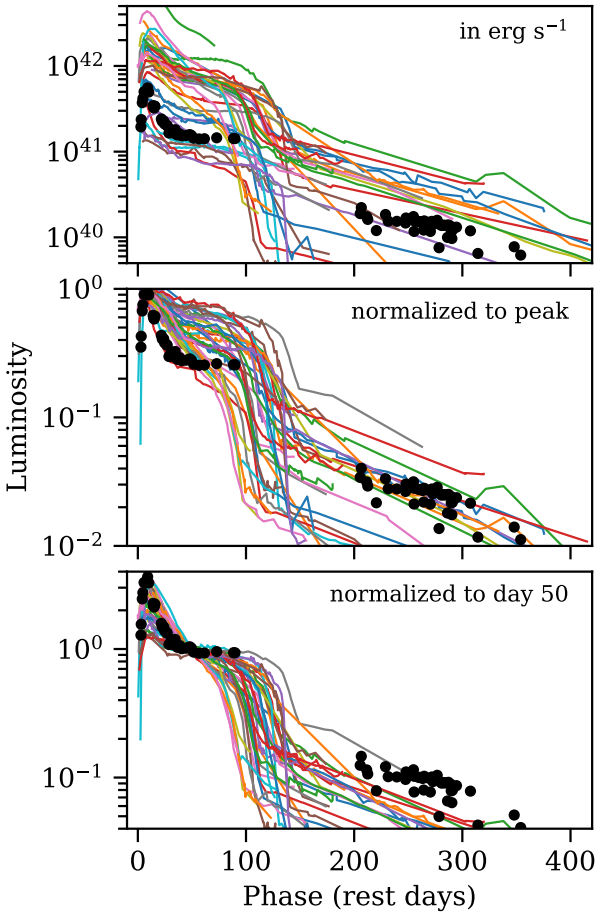

Figure 4. Bolometric light curve of SN 2016bkv (black dots) compared to the Valenti et al. (2016) sample of SNe II (colored lines). SN 2016bkv has among the most extreme initial decline slopes and the smallest fall from plateau.

ature and radius from the fit. The temperature evolution shows an unexpected rise during the first six days. Because we lack photometry blueward of U, the blackbody fits are not strongly constrained at these early times, when the spectral energy distribution peaks in the ultraviolet. If this rising behavior is real, it might be related to the flash ionization of the CSM, which manifests itself in the spectra during the same time period. However, given the uncertainties in the fits, we cannot claim to have observed a significant effect.

4.3. *Shock Cooling Model Fitting*

Sapir & Waxman (2017) present a method for modeling early supernova light curves powered by shock cooling emission—the radiation of energy deposited in the stellar envelope by the core-collapse shock wave. Here we test whether their models alone can reproduce the unusually sharp peak of SN 2016bkv or whether another power source is needed.

We fit our multiband light curve up to MJD 57485.0 (16.3 d after estimated explosion) to the Sapir & Waxman model, with $n = 1.5$ for a RSG, using a Markov-chain Monte Carlo routine, resulting in posterior probability distributions of five parameters: the shock speed, v_{s*}; the mass of the progenitor envelope, M_{env}; the product of a numerical factor that describes the inner envelope structure, f_ρ, and the total ejected mass, M; the progenitor radius, R; and the time of explosion, t_0. For each set of these parameters, the model gives the blackbody temperature and radius as a function of time, which we then convert to magnitudes for each observed photometry point, simultaneously fitting all bands. Figure 6 shows the light curve fits, posterior probability distributions, and 1σ credible intervals centered on the medians. Sapir & Waxman's models are valid when $k_B T > 0.7$ eV, corresponding to a cutoff phase of 25 d after explosion for our best-fit parameters.

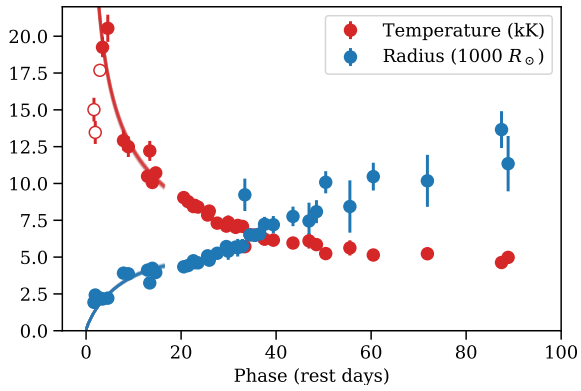

Figure 5. Best-fit blackbody temperature (red points) and radius (blue points) of SN 2016bkv during the photospheric phase, compared to the temperature (red lines) and radius (blue lines) from the best-fit Sapir & Waxman (2017) models in Section 4.3. The open red points are likely underestimates of the temperature from when the SED peaks blueward of our observations.

Using Sapir & Waxman's approximation to f_ρ, we can disentangle the total ejected mass from f_ρ:

$$f_\rho M \approx \sqrt{\frac{M_{env}}{M - M_{env}}} M$$

This gives $M \approx 2.6\,M_\odot$ and $f_\rho \approx 0.48$. We then estimate the ratio of the explosion energy to the ejected mass using approximation of Matzner & McKee (1999), keeping in mind that the result depends on the previous approximation as well:

$$\frac{E}{M} \approx 0.907 f_\rho^{0.382} v_{s*}^2 = 3.0 \times 10^{49}\,\mathrm{erg}\,M_\odot^{-1}$$

This is slightly higher than for the LL SNe II in the sample of Pumo et al. (2017), but still lower than for their intermediate-luminosity category.

Although the fit appears to converge on an optimal set of parameters (see also Figure 5), the models are not able to reproduce the sharpness of the peak around 8 d

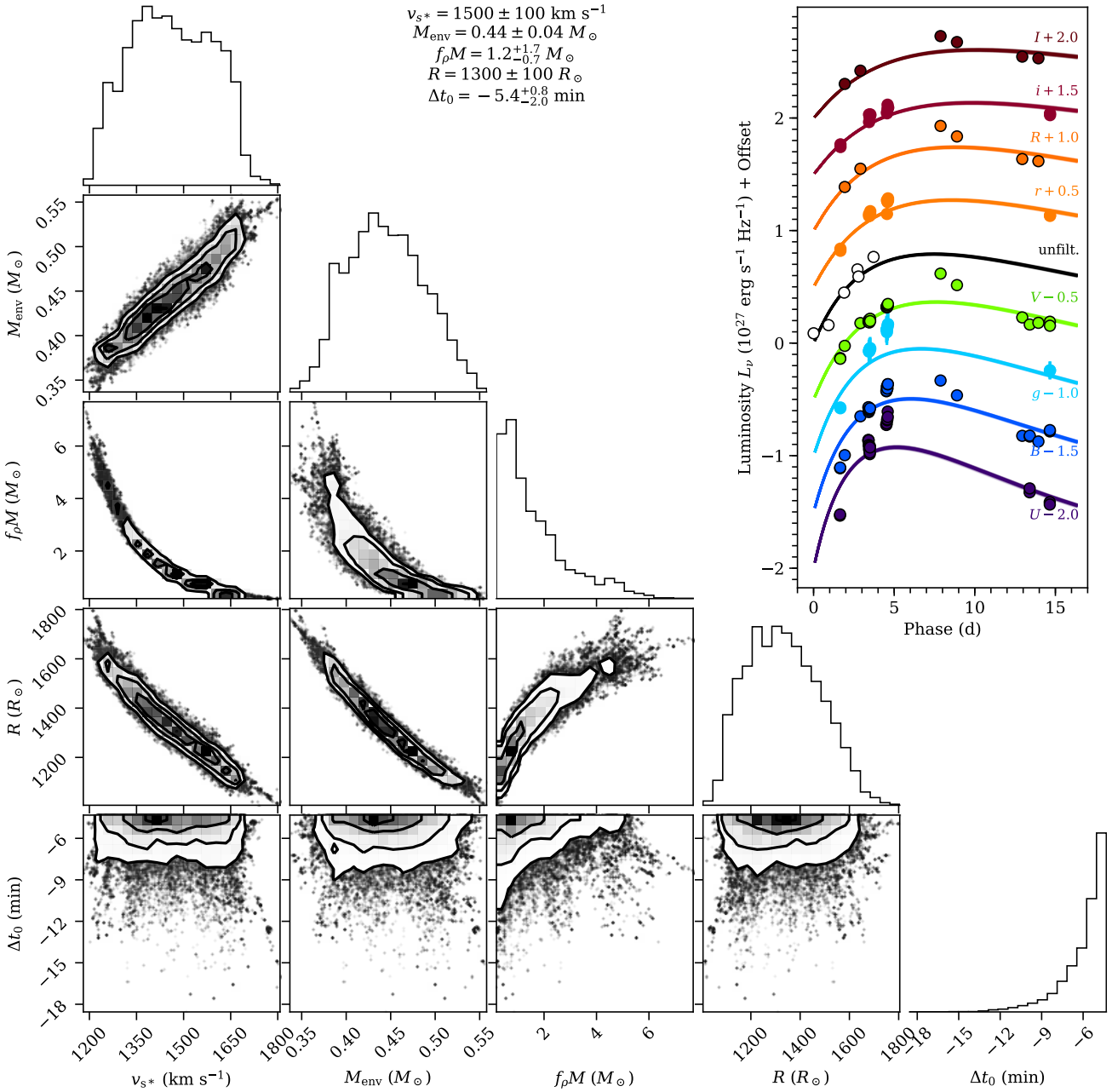

Figure 6. Posterior probability distributions of and correlations between the shock speed, v_{s*}; the mass of the progenitor envelope, M_{env}; the product of a numerical factor that describes the inner envelope structure, f_ρ, and the total ejected mass, M; the progenitor radius, R; and the time between explosion and discovery, Δt_0. The 1σ credible intervals centered around the median are given at the top. The top-right panel shows 100 fits randomly drawn from our MCMC routine compared to the data. (The fits appear to be single lines because the spread in the parameters is small.) We do not consider the shock cooling models to be a good fit to the light curve peak, leaving circumstellar interaction as the most probable power source.

after explosion. This may be evidence that ejecta-CSM interaction contributes significant luminosity in the week around maximum light, which we might expect given our observation of the presence of CSM through flash spectroscopy. Indeed, Morozova et al. (2017a,b) have shown that numerical light curve models that include CSM reproduce these bumps much more faithfully than those with no CSM. In fact, there may be a correlation between the strength of the flash spectroscopy features and the luminosity in the initial light curve peak, but more events with both types of measurements are needed to investigate such a correlation further.

4.4. *Spectral Modeling*

Because of their low photospheric velocities, LL SNe IIP provide a good opportunity to identify which

elements contribute to their photospheric spectra. To aid in this identification, we use SYN++ (Thomas et al. 2011) to produce a synthetic spectrum that resembles our observed spectrum from 34.7 days after explosion. We chose this spectrum because it has a high signal-to-noise ratio, and many strong P Cygni lines are visible. Figure 7 compares the synthetic and observed spectra. The synthesis parameters are listed in the SYN++ input file, which is available in the online journal.

At this phase, the blue half of the optical spectrum is dominated by iron and titanium lines. These two elements plus calcium, sodium, and hydrogen can account for nearly all of the observed features. The most notable feature of our result is that the range of input velocities necessary to reproduce the observed spectrum is only 100–2000 km s^{-1}. Likewise, the photospheric velocity is 1000 km s^{-1}. Since this is near the resolution of our spectrograph, the true ejecta velocity may be lower. The photospheric temperature of our model is 7500 K, close to the blackbody temperature we calculate for this phase in Section 4.2, and the ion temperatures of 10^4 K are reasonable for the interior of the ejecta (although the synthetic spectrum is not very sensitive to these parameters).

Although the line positions match the observed spectrum quite well, a quadratic warping function is necessary to suppress the blue end of the model to match the observations. This function has no physical basis, but deviations from a perfect blackbody continuum with no electron scattering are conceivable. Another possibility is that our spectrograph has lost some of the blue light from the supernova in a way we have not sufficiently accounted for.

4.5. *Nebular Spectra*

Nebular spectra, taken after the ejecta are mostly transparent to optical light, provide several clues about the progenitor structure. We obtained four late-time spectra of SN 2016bkv, from 257 to 607 d after explosion. In Figure 8, we compare these to the nebular spectral models of Jerkstrand et al. (2017) for a 9 $M_\odot$ RSG progenitor. Each observed spectrum has been scaled by a constant factor to match an extrapolation of the r- and i-band photometry. The model spectra have been scaled to match the nickel luminosity of SN 2016bkv at the observed phase.

Our first observed spectrum still shows significant absorption components of some lines, meaning it may not be fully nebular. This observation is consistent with the low velocities observed during the photospheric phase of SN 2016bkv; because the ejecta expand so slowly, they take longer to become optically thin. Note also that the Hβ and Hγ lines may be contaminated by the underlying H II region. However, by 435 d after explosion, the observed and model spectra are in good agreement. We take this as an indication that SN 2016bkv likely comes from a low-mass RSG progenitor. By 607 d after explosion, the observed spectrum is significantly fainter than the model, perhaps due to dust formation in the ejecta.

Although Jerkstrand et al. do not model an electron-capture supernova, they expect nebular spectra from such an explosion would have weaker emission in the following lines: Mg I], [O I], He I, [C I], and O I. These lines are indeed weak in our spectra of SN 2016bkv, with the exception of O I 844.6 nm, which is stronger than the models. As such, we cannot rule out the possibility that SN 2016bkv is an electron capture supernova, although this conclusion is far from certain. An important caveat is that electron-capture supernovae are expected to yield very little radioactive nickel, in stark contrast to our observations in Section 4.2. More observations and further modeling of LL SNe IIP in the nebular phase will be critical to understanding which, if any, supernovae are caused by electron capture.

5. CONCLUSIONS

Two lines of evidence point to strong but short-lived circumstellar interaction in SN 2016bkv. First, flash spectroscopy during the first five days reveals the presence of material around the progenitor star. A few days later, the light curve shows a strong peak as the ejecta interact with this material, adding luminosity on top of the plateau powered by recombination of the hydrogen envelope. This peak cannot be fit with shock cooling models alone. Even with this strong early peak at $M_V = -16$, SN 2016bkv is the lowest-luminosity supernova to show flash ionization lines, suggesting that late-stage mass loss is common even among low-mass RSGs.

SN 2016bkv is also exceptional in its short fall from plateau, indicating a large nickel production (0.022 $M_\odot$) compared to other LL SNe II. Despite this, our analysis of the nebular spectrum suggests it came from a low-mass ($\sim 9\,M_\odot$) RSG progenitor, in agreement with the 8 to 15 $M_\odot$ progenitors for LL SNe II observed with *HST*. Certain emission lines in these spectra hint at the possibility of SN 2016bkv being an electron-capture supernova, although we cannot yet definitively distinguish between this case and the traditional iron core-collapse model.

This and other work suggests that analyses of SNe II should be careful to distinguish between the properties of the progenitor star itself and the properties of its circumstellar environment. Peak luminosity, for example, can be strongly affected by circumstellar interaction, whereas luminosity after settling on the plateau may be related to the intrinsic properties of the star. Future data sets like the one presented here, with early and

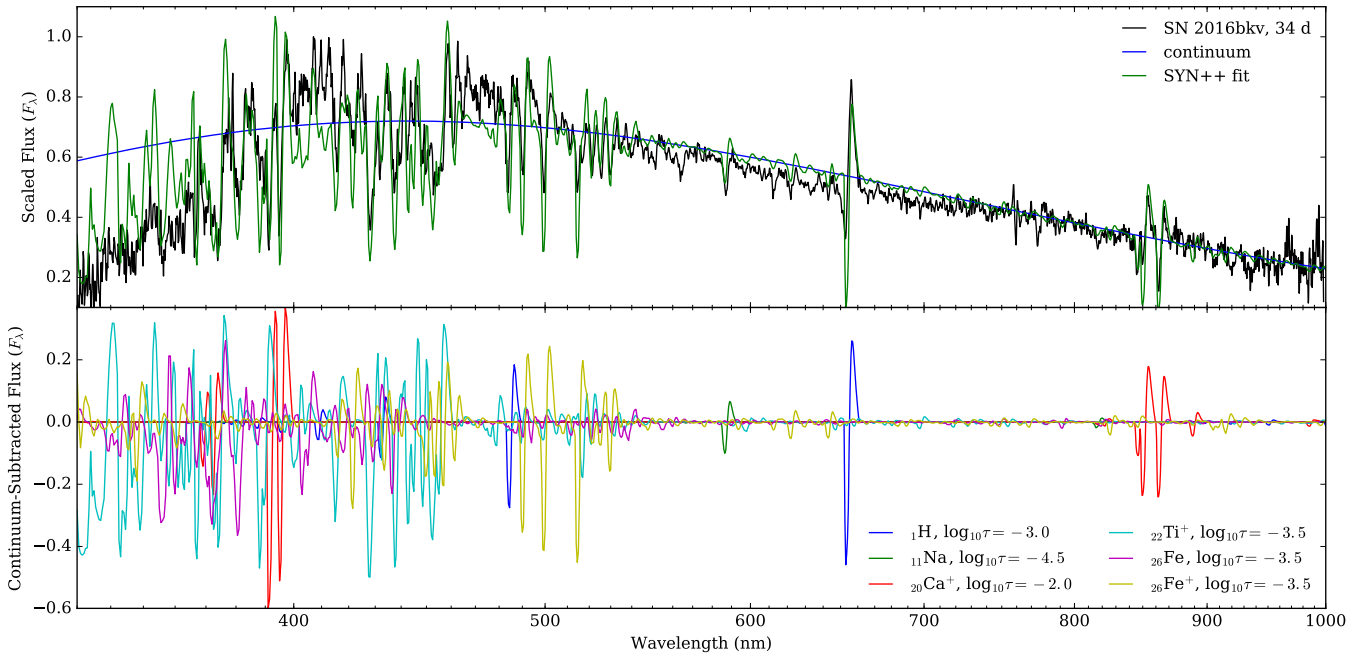

Figure 7. SYN++ model for the spectrum of SN 2016bkv 34.7 days after maximum light. The top panel shows the observed spectrum, the assumed continuum (a 7500 K blackbody warped by a quadratic polynomial; see Section 4.4), and the total synthetic spectrum (also warped). The bottom panel shows the contributions to the synthetic spectrum of each of the six ions we consider. (The SYN++ input file used to create this figure is available.)

long-term coverage of young supernovae, will allow us to constrain progenitor properties and mass-loss history separately, by comparing to numerical light-curve and spectral models.

We thank Nir Sapir for his advice on fitting the shock cooling models and Rollin Thomas for his help using SYN++. We are grateful to the staff at the Keck Observatory for their assistance. The W. M. Keck Observatory is operated as a scientific partnership among the California Institute of Technology, the University of California, and NASA; it was made possible by the generous financial support of the W. M. Keck Foundation. Research at Lick Observatory is partially supported by a generous gift from Google.

G.H., C.M., and D.A.H. are supported by the National Science Foundation under grant No. 1313484. Support for I.A. was provided by NASA through the Einstein Fellowship Program. X.W. is supported by the National Natural Science Foundation of China (NSFC grants 11325313 and 11633002). This work was also partially Supported by the Open Project Program of the Key Laboratory of Optical Astronomy, National Astronomical Observatories, Chinese Academy of Sciences. G.H. is an LSSTC Data Science Fellow.

Facilities: ADS, Beijing:0.8m, Beijing:2.16m (BFOSC, OMR), Keck:I (LRIS), LCOGT (FLOYDS, Sinistro), NED, Shane (Kast)

Software: Astropy (Astropy Collaboration 2013), `emcee` (Foreman-Mackey et al. 2013), HOTPANTS (Becker 2015), `lcogtsnpipe` (Valenti et al. 2016), PyRAF (Science Software Branch at STScI 2012), PyZOGY (Guevel & Hosseinzadeh 2017), SExtractor (Bertin & Arnouts 1996), SYN++ (Thomas et al. 2011)

REFERENCES

Adelman-McCarthy, J. K., Allam, S. S., Allende Prieto, C., et al. 2007, ApJS, 175, 297

Aihara, H., Allende Prieto, C., An, D., et al. 2011, ApJS, 193, 29

Albareti, F. D., Prieto, C. A., Almeida, A., et al. 2017, ApJS, 233, 25

Arcavi, I. 2017, in Handbook of Supernovae, ed. A. W. Alsabti & P. Murdin (Berlin: Springer), in press

Astropy Collaboration, Robitaille, T. P., Tollerud, E. J., et al. 2013, A&A, 558, A33

Barbon, R., Buondi, V., Cappellaro, E., & Turatto, M. 2008, yCat, 1, 2024

Barbon, R., Ciatti, F., & Rosino, L. 1979, A&A, 72, 287

Becker, A. 2015, HOTPANTS: High Order Transform of PSF ANd Template Subtraction, ASCL, http://ascl.net/1504.004

Benetti, S., Patat, F., Turatto, M., et al. 1994, A&A, 285, L13

Bertin, E., & Arnouts, S. 1996, A&AS, 117, 393

Brown, T. M., Baliber, N., Bianco, F. B., et al. 2013, PASP, 125, 1031

Chugai, N. N. 1991, MNRAS, 250, 513

Chugai, N. N., & Utrobin, V. P. 2000, A&A, 354, 557

Fan, Z., Wang, H., Jiang, X., et al. 2016, PASP, 128, 115005

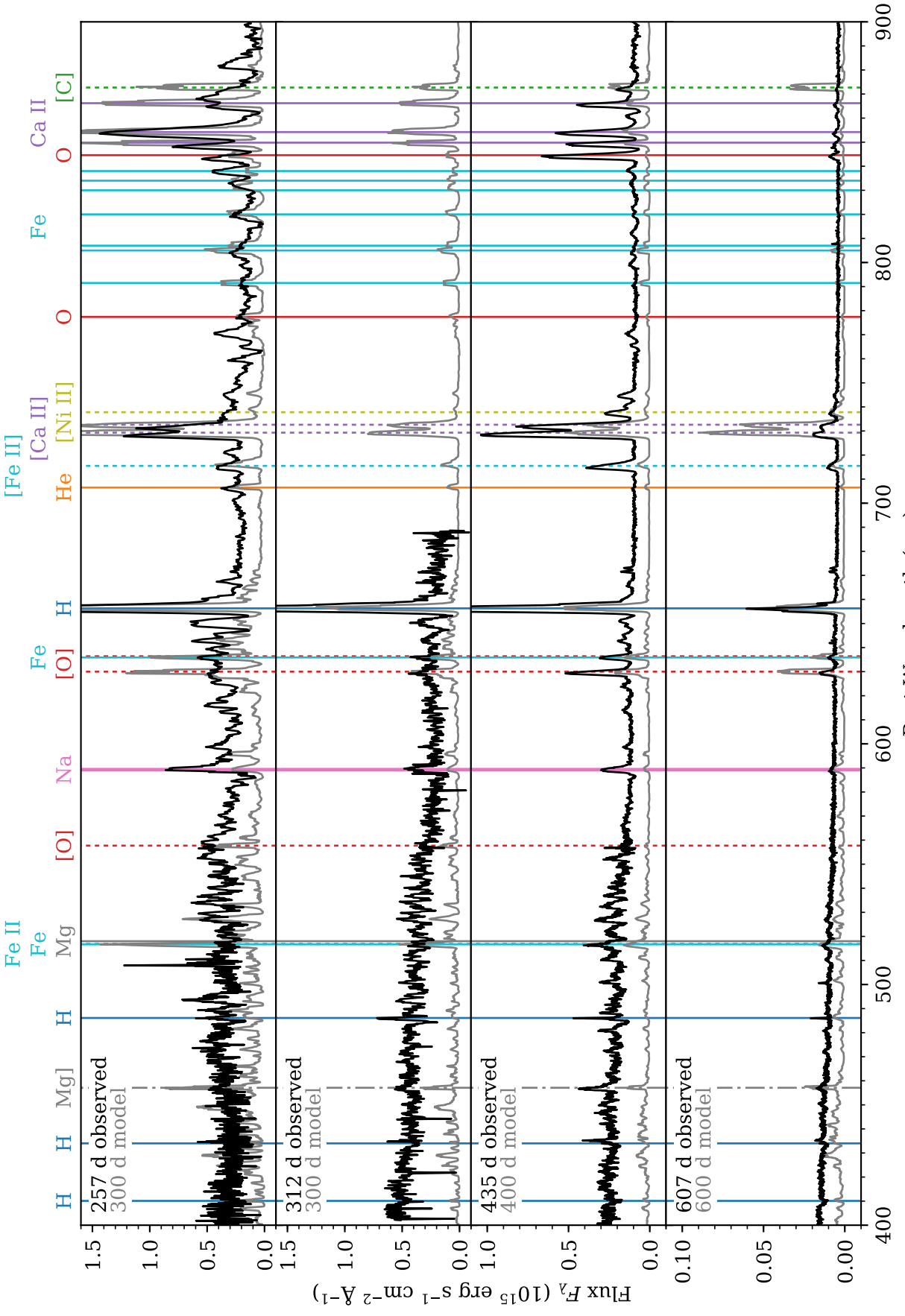

Figure 8. Late-time spectra of SN 2016bkv compared to the 9 $M_\odot$ model of Jerkstrand et al. (2017). The observed spectra are calibrated to extrapolated r- and i-band photometry, and the model spectra are scaled to match the nickel mass and phase of the observed spectra. SN 2016bkv evolves more slowly than the model; our first spectrum still shows absorption lines, meaning it is not fully nebular. However, the agreement at 400 d suggests SN 2016bkv may come from a low-mass progenitor.

Faran, T., Poznanski, D., Filippenko, A. V., et al. 2014, MNRAS, 442, 844
Ferrarese, L., Mould, J. R., Kennicutt, R. C., et al. 1999, ApJ, 529, 745
Foreman-Mackey, D., Hogg, D. W., Lang, D., & Goodman, J. 2013, PASP, 125, 306
Gal-Yam, A., Kasliwal, M. M., Arcavi, I., et al. 2011, ApJ, 736, 159
Gal-Yam, A., Arcavi, I., Ofek, E. O., et al. 2014, Natur, 509, 471
Garnavich, P. M., & Ann, H. B. 1994, AJ, 108, 1002
Groh, J. H. 2014, A&A, 572, L11
Guevel, D., & Hosseinzadeh, G. 2017, PyZOGY, v.0.0.1, Zenodo, doi:10.5281/zenodo.1043973
Hamuy, M. 2003, ApJ, 582, 905
Hamuy, M., & Pinto, P. A. 2002, ApJ, 566, L63
Hodge, P. W., & Kennicutt, Jr., R. C. 1983, AJ, 88, 296
Hosseinzadeh, G., Howell, D. A., Arcavi, I., McCully, C., & Valenti, S. 2016, ATel, 8859, 1
Huang, F., Li, J.-Z., Wang, X.-F., et al. 2012, RAA, 12, 1585
Itagaki, K. 2016, TNSTR, 234, 1
Jerkstrand, A., Ertl, T., Janka, H.-T., et al. 2017, arXiv:1710.04508
Jones, M. I., Hamuy, M., Lira, P., et al. 2009, ApJ, 696, 1176
Khazov, D., Yaron, O., Gal-Yam, A., et al. 2016, ApJ, 818, 3
Landolt, A. U. 1992, AJ, 104, 340
Leonard, D. C., Filippenko, A. V., Barth, A. J., & Matheson, T. 2000, ApJ, 536, 239
Li, W., Van Dyk, S. D., Filippenko, A. V., et al. 2006, ApJ, 641, 1060
Matheson, T., Filippenko, A. V., Chornock, R., Leonard, D. C., & Li, W. 2000, AJ, 119, 2303
Matzner, C. D., & McKee, C. F. 1999, ApJ, 510, 379
Maund, J. R., Smartt, S. J., & Danziger, I. J. 2005, MNRAS, 364, L33
Milisavljevic, D., Chilingarian, I., Berlind, P., et al. 2016, ATel, 8861, 1
Miller, J. S., & Stone, R. P. S. 1994, The Kast Double Spectograph, Lick Observatory Technical Reports No. 66 (Santa Cruz: Lick Observatory)
Morozova, V., Piro, A. L., & Valenti, S. 2017a, arXiv:1709.04928
—. 2017b, ApJ, 838, 28
Niemela, V. S., Ruiz, M. T., & Phillips, M. M. 1985, ApJ, 289, 52
Oke, J. B., Cohen, J. G., Carr, M., et al. 1995, PASP, 107, 375
Pastorello, A., Zampieri, L., Turatto, M., et al. 2004, MNRAS, 347, 74
Pastorello, A., Sauer, D., Taubenberger, S., et al. 2006, MNRAS, 370, 1752
Patat, F., Barbon, R., Cappellaro, E., & Turatto, M. 1994, A&A, 282, 731
Pejcha, O., & Prieto, J. L. 2015, ApJ, 806, 225
Pierce, M. J. 1994, ApJ, 430, 53
Pumo, M. L., Zampieri, L., Spiro, S., et al. 2017, MNRAS, 464, 3013
Quimby, R. M., Wheeler, J. C., Höflich, P., et al. 2007, ApJ, 666, 1093
Rockosi, C., Stover, R., Kibrick, R., et al. 2010, SPIE, 7735E, 0R
Ross, T. W., Channa, S., Molloy, J. D., Zheng, W., & Filippenko, A. V. 2016, ATel, 8875, 1
Sapir, N., & Waxman, E. 2017, ApJ, 838, 130
Schlegel, E. M. 1990, MNRAS, 244, 269
—. 2001, ApJ, 556, L25
Science Software Branch at STScI. 2012, PyRAF: Python alternative for IRAF, ASCL, http://ascl.net/1207.011
Shapley, H. 1939, PNAS, 25, 569
Shivvers, I., Groh, J. H., Mauerhan, J. C., et al. 2015, ApJ, 806, 213
Smartt, S. J. 2009, ARA&A, 47, 63
Smartt, S. J., Gilmore, G. F., Trentham, N., Tout, C. A., & Frayn, C. M. 2001, ApJ, 556, L29
Smith, N., Li, W., Silverman, J. M., Ganeshalingam, M., & Filippenko, A. V. 2011, MNRAS, 415, 773
Spiro, S., Pastorello, A., Pumo, M. L., et al. 2014, MNRAS, 439, 2873
Strauss, M. A., Huchra, J. P., Davis, M., et al. 1992, ApJS, 83, 29
Thomas, R. C., Nugent, P. E., & Meza, J. C. 2011, PASP, 123, 237
Turatto, M., Mazzali, P. A., Young, T. R., et al. 1998, ApJL, 498, L129
Valenti, S., Howell, D. A., Stritzinger, M. D., et al. 2016, MNRAS, 459, 3939
Yaron, O., & Gal-Yam, A. 2012, PASP, 124, 668
Yaron, O., Perley, D. A., Gal-Yam, A., et al. 2017, NatPh, 13, 510
Zackay, B., Ofek, E. O., & Gal-Yam, A. 2016, ApJ, 830, 27
Zampieri, L., Shapiro, S. L., & Colpi, M. 1998, ApJL, 502, L149